Surface effects in simulations of scanning electron microscopy images

Van Kessel, L.; Hagen, C. W.; Kruit, P.

DOI
10.1117/12.2514824

Publication date
2019

Document Version
Final published version

Published in
Proceedings of SPIE

Surface effects in simulations of scanning electron microscopy images

van Kessel, L., Hagen, C., Kruit, P.

L. van Kessel, C. W. Hagen, P. Kruit, "Surface effects in simulations of scanning electron microscopy images," Proc. SPIE 10959, Metrology, Inspection, and Process Control for Microlithography XXXIII, 109590V (26 March 2019); doi: 10.1117/12.2514824

SPIE.

Event: SPIE Advanced Lithography, 2019, San Jose, California, United States

Surface effects in simulations of scanning electron microscopy images

L. van Kessel[a], C.W. Hagen[a], and P. Kruit[a]

[a]Delft University of Technology, Dept. Imaging Physics, Lorentzweg 1, 2628 CJ Delft, The Netherlands

ABSTRACT

We have investigated the contributions of surface effects to Monte Carlo simulations of top-down scanning electron microscopy (SEM) images. The elastic and inelastic scattering mechanisms in typical simulations assume that the electron is deep in the bulk of the material. In this work, we correct the inelastic model for surface effects. We use a model for infinite flat surfaces, and apply it to non-flat, but smooth, geometries. Though this is a simplification, it captures most qualitative differences to the bulk model, including coupling to surface plasmons. We find that this correction leads to an increased SE signal near a feature's sidewall in low-voltage critical dimension SEM (CD-SEM). The effect is strongest for low beam energies. Due to some of the assumptions in our model, we are unable to quantitatively predict the extent by which the signal from the sidewall is enhanced. The enhancement of signal from the sidewall may be large enough to cause the measured edge position to shift significantly.

Keywords: Surface plasmons, Scanning electron microscopy, Monte Carlo simulation

1. INTRODUCTION

Scanning electron microscopy is a standard tool for the inspection of semiconductor devices. It involves a focused electron beam scanning over a sample. The beam–sample interaction is a nontrivial process, producing secondary electrons (SEs) in a finite-sized interaction volume as well as backscattered electrons (BSEs). The interpretation of a SEM image is fairly straightforward if the features are large, but details of the beam-sample interaction become increasingly important as device features continue to shrink.

Semi-analytical models for the SEM signal have been proposed,[1,2] but the most rigorous method in current use is Monte Carlo simulations.[3–6] These simulations attempt to predict the SEM image, assuming the sample geometry and material composition are known exactly. Starting from physical principles, they make broadly similar assumptions. An electron is treated as a classical point particle, scattering through the volume of a material in discrete events. The electron is treated as if it is in free flight between such events. The scattering probability per unit distance travelled, $p(x)$, is given by an exponential distribution,

$$p(x) = \frac{1}{\lambda} e^{-x/\lambda}, \tag{1}$$

where λ is called the mean free path.

Two independent types of scattering are typically distinguished: elastic scattering, where an electron changes direction without losing energy; and inelastic scattering, where an electron loses energy and may excite a secondary electron. Each of these mechanisms has its own mean free path. In addition, as an electron reaches a material interface, it may be reflected or refracted due to the change of inner potential between the materials.

The reflection and refraction of electrons at a surface is only one of the many effects that play a role at an interface. For example, there may be oxidation layers, dangling bonds and contamination. Such highly sample-dependent effects are not considered in this work.

E-mail: L.C.P.M.vanKessel@tudelft.nl
E-mail: C.W.Hagen@tudelft.nl

Metrology, Inspection, and Process Control for Microlithography XXXIII, edited by Vladimir A. Ukraintsev, Ofer Adan, Proc. of SPIE Vol. 10959, 109590V © 2019 SPIE · CCC code: 0277-786X/19/$18 · doi: 10.1117/12.2514824

An assumption that is often tacitly made, is that elastic and inelastic scattering always behave as if the electron is deep inside bulk material. This assumption is already present in equation (1), because the mean free path (and hence the scattering probability) does not depend on the location of the electron. For scattering mechanisms that can be well described by electrons scattering on isolated atoms, such as inner-shell excitation or elastic Mott scattering, this is a valid approximation. For events where the electron probes the solid-state bulk, such as electron–phonon scattering or plasmon excitation, we may expect scattering behaviour to be different near an interface.

Indeed, coincidence measurements performed in transmission electron microscopes[7–9] have provided evidence that surface plasmons may contribute significantly to SE emission. Werner *et al.*[10] performed a similar study in aluminium, at a beam energy (100 eV) close to low-voltage SEM. They find clear evidence for the contribution of surface plasmon decay to SE emission, of similar magnitude to the volume plasmon. Neglecting surface plasmons in simulations of SEM images, as is typically done, may therefore not be acceptable.

In the present work, we follow a framework similar to previous simulations of SEM images. However, we replace the inelastic scattering mechanism by one where the material interface is explicitly taken into account. This dielectric formalism includes surface plasmons as well as the "Begrenzung" effect, the reduced coupling strength to the volume plasmon near an interface. The goal of the present work is to study the sensitivity of simulated SEM images to the inclusion of these effects.

We briefly mention the elastic and boundary scattering models used in section 2. These are similar to what is currently in common use. Surface plasmons are introduced by replacing the inelastic scattering model. This is discussed in detail in section 3. Results are shown in section 4.

2. SCATTERING MODELS

For the energy range above 200 eV, we use Mott elastic scattering.[11] These scattering cross sections are obtained by solving the Dirac equation in a model potential near an atom. We use the ELSEPA program by Salvat *et al.*[12] to compute these scattering cross sections.

For energies lower than approximately 100 eV, the Mott description breaks down. As pointed out by Kieft *et al.*,[4] the electron's wavelength becomes comparable to interatomic distances. The picture of an electron scattering on a single isolated atom is no longer valid. A more technical issue is that the Mott scattering cross section becomes heavily dependent on assumptions in the model potential. Similarly to Kieft *et al.*, we use electron–acoustic phonon scattering for energies lower than 100 eV, based on the work of Schreiber *et al.*[13] In the range 100 eV to 200 eV, we interpolate between acoustic phonon and Mott scattering.

As an electron crosses a material interface, it probes the difference of inner potential between the materials. This may cause the electron to be reflected, or transmitted and refracted. We use a simple step function model potential to determine the transmission coefficient.

3. SURFACE FORMALISM

Typical modern simulations use the dielectric function to describe the inelastic scattering of electrons in matter. The strength of this approach is that the dielectric function can be measured in the optical regime. Assuming that all of space is occupied by a material with dielectric function $\epsilon(q,\omega)$, and that the electron is a single point charge, Maxwell's equations can be solved to find the induced electric field in the material. This electric field is oriented such that it slows down the electron, which is interpreted as inelastic scattering.

The result is an inelastic mean free path given by the famous equation

$$\lambda^{-1} = \frac{1}{\pi a_0 E} \int \mathrm{d}\omega \int \frac{\mathrm{d}q}{q} \ \mathrm{Im}\left[\frac{-1}{\epsilon(q,\omega)}\right]. \tag{2}$$

Here, ω represents the energy loss, q is the momentum transferred, E is the primary electron's kinetic energy before the collision and a_0 is the Bohr radius. Integration is over the kinematically allowed range. Probability densities for energy and momentum loss are given by $\lambda\frac{\partial\lambda^{-1}}{\partial\omega}$ and $\lambda\frac{\partial\lambda^{-1}}{\partial q}$, respectively.

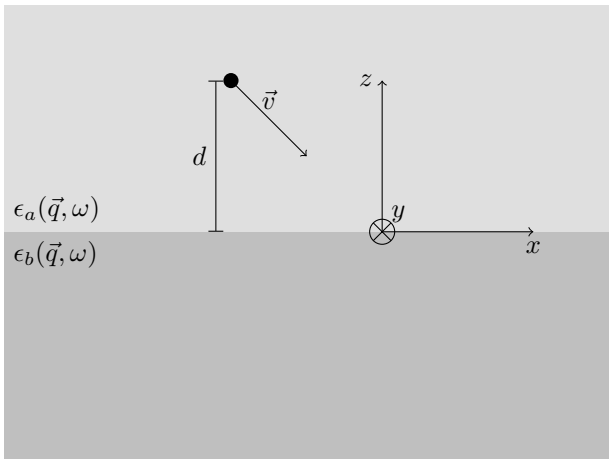

Figure 1. Geometry used by Salvat-Pujol *et al.*. Shaded areas represent the two materials, represented by dielectric functions $\epsilon_a(\vec{q},\omega)$ and $\epsilon_b(\vec{q},\omega)$. They are separated by the $z = 0$ plane. The electron moves with velocity $\vec{v}$ and passes through the origin at time $t = 0$.

In the general case, when not all of space is occupied by the same material, a similar analysis can be performed. However, the technicalities of solving the electric field are much more complicated. This has been done analytically for simple geometries,[14] such as infinite flat surfaces, wedges, or spheres.

For structures relevant to lithography, finding analytical solutions is impractical or impossible. A physically accurate alternative would involve numerically solving the induced electric field for every electron position, direction and energy of interest. This parameter space is prohibitively large.

Instead, we make the following simplification. We use the analytically known solution for infinite flat surfaces, and apply it to arbitrary geometries assuming that the radius of curvature in the geometry is sufficiently large everywhere. We will investigate the meaning of "sufficiently large" in more detail later.

We use the results from Salvat-Pujol *et al.*[15] A full derivation is given in that reference, we only repeat the main results. The situation is illustrated in figure 1. Materials with dielectric functions $\epsilon_a(\vec{q},\omega)$ and $\epsilon_b(\vec{q},\omega)$ fill the spaces $z > 0$ and $z < 0$, respectively. The electron moves with velocity $\vec{v}$. The electron's z coordinate is denoted as d, positive for region a and negative for region b. At time $t = 0$, the electron passes through the origin.

Salvat-Pujol *et al.* solve this situation for a non-relativistic electron by means of the image charge method. The assumption that the electron is not relativistic makes the problem formally electrostatic. Salvat-Pujol *et al.* remark that the usual boundary conditions for the electric and displacement fields at $z = 0$ are not restrictive enough to uniquely determine the image charges. Previous literature has chosen a variety of image charges to investigate the non-relativistic case. Salvat-Pujol *et al.* parameterise the choice for image charges by the tuple of numbers (p_1, p_2, p_3), which can be set to $(0, 1, 0)$ or $(1, 1, 1)$ to reproduce earlier literature results.

The result is an inverse mean free path consisting of a bulk and a surface term: $\lambda^{-1} = \lambda_B^{-1} + \lambda_S^{-1}$. The surface term captures both the surface plasmon coupling as well as the "Begrenzung" of the volume plasmon. The bulk term, λ_B^{-1}, is similar to equation (2), where ϵ_a or ϵ_b is selected depending on the sign of d. The surface interaction is given by

$$\begin{aligned}\lambda_S^{-1} = &-\frac{\hbar}{m_e a_0 \pi^2}\frac{|v_z|}{v}\int_0^{E/\hbar}\mathrm{d}\omega\int_{q_-}^{q_+}\mathrm{d}q\int_0^{\pi}\mathrm{d}\theta\,\sin\theta\int_0^{2\pi}\mathrm{d}\phi\,\frac{1}{q_\parallel^2 v_z^2 + \left(\omega - \vec{q}_\parallel\cdot\vec{v}_\parallel\right)^2}\\ &\times\left[\Theta(-t)e^{-q_\parallel|d|} + \Theta(t)\left(2\cos\left\{(\omega-\vec{q}_\parallel\cdot\vec{v}_\parallel)t\right\} - e^{-q_\parallel|d|}\right)\right]\\ &\times\mathrm{Im}\left[e^{iq_z d}f(\vec{q}_\parallel,\omega)\left\{\frac{\Theta(d)}{\epsilon_a(\vec{q},\omega)} - \frac{\Theta(-d)}{\epsilon_b(\vec{q},\omega)}\right\}\right].\end{aligned} \tag{3}$$

We use the notation that any vector $\vec{a}$ has components $\vec{a} = (a_x, a_y, a_z)$, the shorthand $a = |\vec{a}|$, and $\vec{a}_\parallel = (a_x, a_y)$ is the two-dimensional projection oriented parallel to the interface. Furthermore, $\vec{q} = q(\cos\phi\sin\theta, \sin\phi\sin\theta, \cos\theta)$, $\Theta(x)$ is the Heaviside step function, and

$$\frac{\hbar q_\pm}{\sqrt{2m_e}} = \sqrt{E} \pm \sqrt{E-\omega}, \tag{4}$$

$$k_z = \frac{\omega - \vec{q}_\parallel \cdot \vec{v}_\parallel}{v_z}, \tag{5}$$

$$f(\vec{q}_\parallel, \omega) = \frac{\dfrac{p_2}{\epsilon_b(\vec{q}_\parallel, k_z, \omega)} - \dfrac{1}{\epsilon_a(\vec{q}_\parallel, k_z, \omega)} + \dfrac{p_3}{\epsilon_b(\vec{q}_\parallel, -k_z, \omega)} - \dfrac{p_1}{\epsilon_a(\vec{q}_\parallel, -k_z, \omega)}}{\displaystyle\int_{-\infty}^{\infty} \mathrm{d}\kappa \, \frac{1}{q_\parallel^2 + \kappa^2} \left[\frac{1}{\epsilon_a(\vec{q}_\parallel, \kappa, \omega)} + \frac{1}{\epsilon_b(\vec{q}_\parallel, \kappa, \omega)}\right]}. \tag{6}$$

As before, the probability distributions of losing energy ω or momentum $\vec{q}$ are given by $\lambda\frac{\partial\lambda^{-1}}{\partial\omega}$ and $\lambda\frac{\partial\lambda^{-1}}{\partial\vec{q}}$.

We emphasise that λ_S^{-1} cannot be seen separately from λ_B^{-1}. λ_S^{-1} can be negative, representing a reduction in the bulk interaction. The sum $\lambda^{-1} = \lambda_B^{-1} + \lambda_S^{-1}$, however, must be positive.

We also note that λ_S^{-1} changes as the electron travels. λ^{-1} represents the scattering cross section in the electron's immediate environment, which is usually constant between successive events. This is not true in the present case, so λ can no longer be directly interpreted as the mean distance travelled between scattering events.

3.1 Features of the surface correction

A thorough discussion of the physical features contained in the surface formalism is already given by Salvat-Pujol *et al.*[15] For the reader's convenience, we repeat some of the main conclusions. We use the same dielectric function,

$$\frac{1}{\epsilon(q,\omega)} = 1 - \frac{\Omega_p^2}{\hbar^2 Z} \sum_{j=1}^{n} \frac{f_j}{\omega_j^2 + \hbar^2 q^4/4m_e^2 - \omega^2 - i\gamma_j\omega}, \tag{7}$$

with, for aluminium, $Z = 13$, $\Omega_p = 32.84\,\mathrm{eV}$, $n = 1$, $\hbar\omega_1 = 15.01\,\mathrm{eV}$, $f_1 = 3$, $\hbar\gamma_1 = 0.5\,\mathrm{eV}$.

This dielectric function model is considerably simpler than what is usually employed in Monte Carlo simulations. One typically uses measured data in the optical ($q \approx 0$) regime, extended to the $q > 0$ plane by theoretical means. This is likely to yield more accurate results than the present single-oscillator fit. We use a single-oscillator fit for purely practical reasons: (1) it allows a direct comparison to the work of Salvat-Pujol *et al.* and (2) we only have the imaginary part of $1/\epsilon$ available. The real part can be obtained via the Kramers–Kronig relations, which should be done in a full analysis.

We consider an electron normally incident on a flat vacuum–aluminium interface. Figure 2 shows the differential inverse mean free path (DIMFP) with respect to energy, $\partial\lambda^{-1}/\partial\omega$, for a 100 eV electron for several distances d to the interface. In the left figure, the electron is on the vacuum side; in the right figure, it is on the aluminium side.

When the electron is far on the vacuum side, it can't lose any energy. However, as it approaches the interface, a peak appears near 11 eV, aluminium's surface plasmon energy. The surface plasmon coupling increases in strength as the electron closes in on the surface.

As soon as the electron moves to the aluminium side, a second peak appears beside the surface plasmon interaction. This second peak represents the volume plasmon of aluminium. As the electron moves deeper into the material, the surface plasmon coupling decreases in strength while the volume plasmon becomes stronger. This reduction of the volume plasmon coupling near the interface is known as the "Begrenzung" effect. At a depth of 0.5 nm, the DIMFP is very similar to the bulk DIMFP.

Similar effects can be seen for a 500 eV electron (figure 3). For the purposes of this work, we want to note two things. First, the "surface layer" is somewhat thicker. For a 100 eV electron, the surface interaction becomes negligible at less than 5 Å from the interface. This interaction extends further for a 500 eV electron. In general,

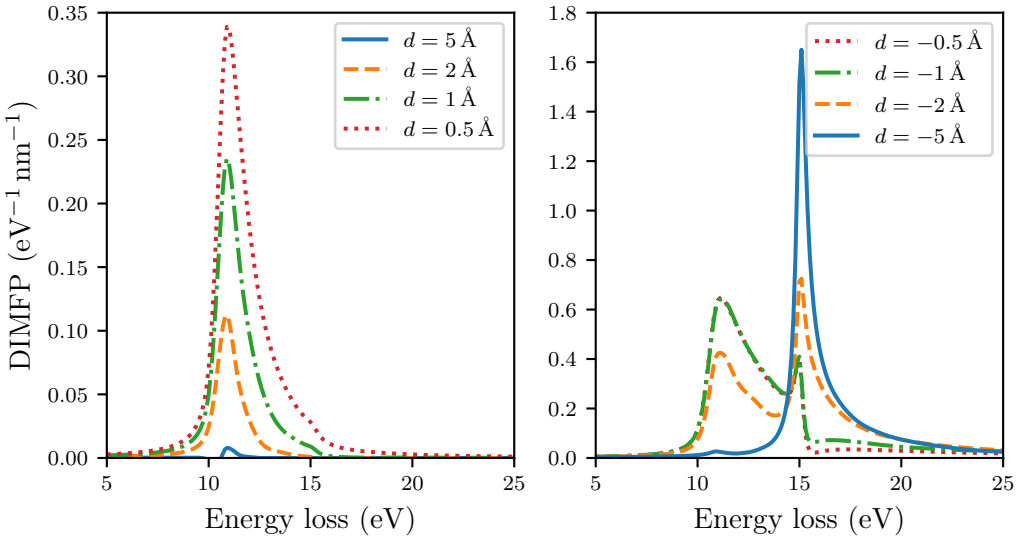

Figure 2. Differential inverse mean free path (DIMFP) for a 100 eV electron, as a function of energy loss ω, for several distances d to a vacuum–aluminium interface. This represents the probability for an electron to lose a certain amount of energy, per unit distance travelled. The electron's direction is oriented from the vacuum towards the aluminium, along the surface normal. In the left figure ($d > 0$), the electron is on the vacuum side; in the right figure, it is on the aluminium side. The $d = -0.5$ Å curve on the right is hidden behind the curve for $d = -1$ Å.

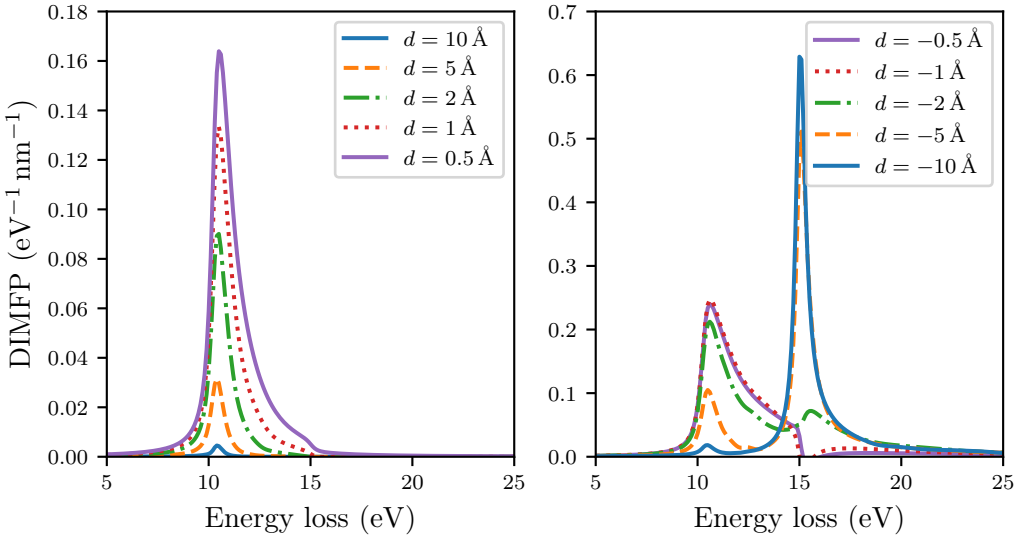

Figure 3. Same as figure 2, for a 500 eV electron.

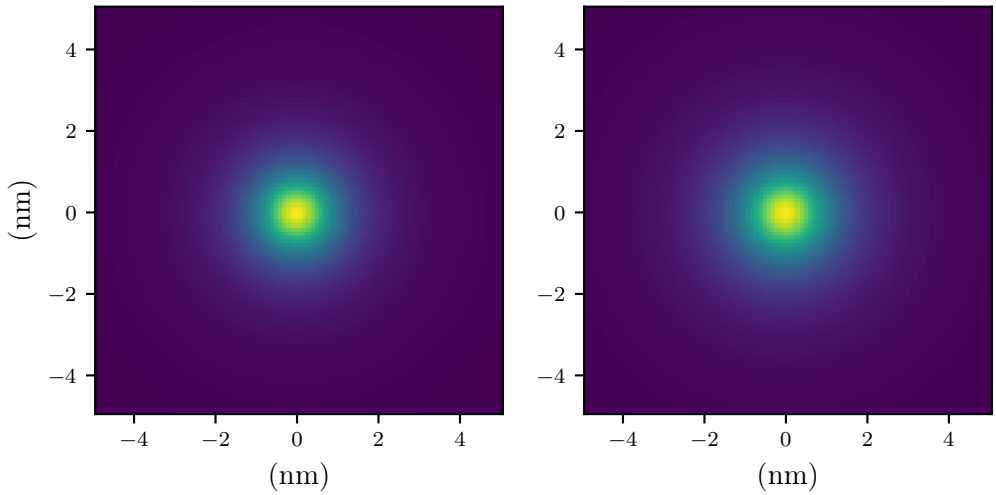

Figure 4. Induced surface charge on a flat aluminium surface, for a 300 eV (left) and 500 eV (right) electron. The electron is 5 Å outside the aluminium, and travels towards the surface along the normal.

the surface layer is thicker for faster electrons. Second, the 500 eV electron has a lower interaction probability per unit distance travelled. This is a familiar effect also observed in bulk mean free paths.

We emphasise the extremely short range in which the surface correction is relevant. Even for 500 eV electrons, the surface layer is less than a nm thick. Figures 2 and 3 show data for distances of 0.5 Å from the surface, much less than the distance between two atoms*. The dielectric function is a continuum approximation to the microscopic response of the material, and whether it is a valid means to treat surface interactions at such small scales (low electron energies) is open for debate.

3.2 Justification of the infinite flat plane approximation

We have assumed that a curved geometry can be approximated as flat, if the curvature is smooth enough. This assumption needs to be justified, which we will do in two ways.

It would be wrong to take the very thin surface layer as a measure for the surface's minimum radius of curvature. Instead, we look at the spatial extent of the induced surface charge. In the work of Salvat-Pujol *et al.*, there are three types of contributions to the electric field: the electron itself, its image charges in the bulk, and the induced surface charge. Clearly, if the geometry curves significantly on a scale where the surface charge is significant, the boundary conditions at the interface are not satisfied and the flat-plane approximation is wrong. Conversely, we may hope that if the interface curves far away from any significant surface charge, the boundary conditions at the interface are still approximately satisfied.

Figure 4 shows the surface charge for 300 eV and 500 eV electrons, each 5 Å outside aluminium, moving directly towards the aluminium. The surface charge can be seen to decay to almost zero within a few nm. When applying the surface formalism to curved geometries, we will use electrons of no more than 500 eV and a radius of curvature of at least 5 nm.

More justification comes from a numerical comparison to an analytical result for a curved geometry. García de Abajo[14] gives analytical expressions for several geometries. We choose the case of an electron passing outside a spherical nanoparticle.

It is well-established that surface plasmons on spherical nanoparticles can behave qualitatively differently than on a flat plane. For a flat metallic plane in vacuum, the surface plasmon energy $\omega_s = \omega_p/\sqrt{2}$, where ω_p is the bulk plasmon energy. A nanosphere, however, can support a large spectrum of modes between $\omega_p/\sqrt{3}$ and $\omega_p/\sqrt{2}$. High-energy (of order 100 keV) electrons dominantly excite the low-order modes.

*Salvat-Pujol *et al.*[15] dare to go even lower.

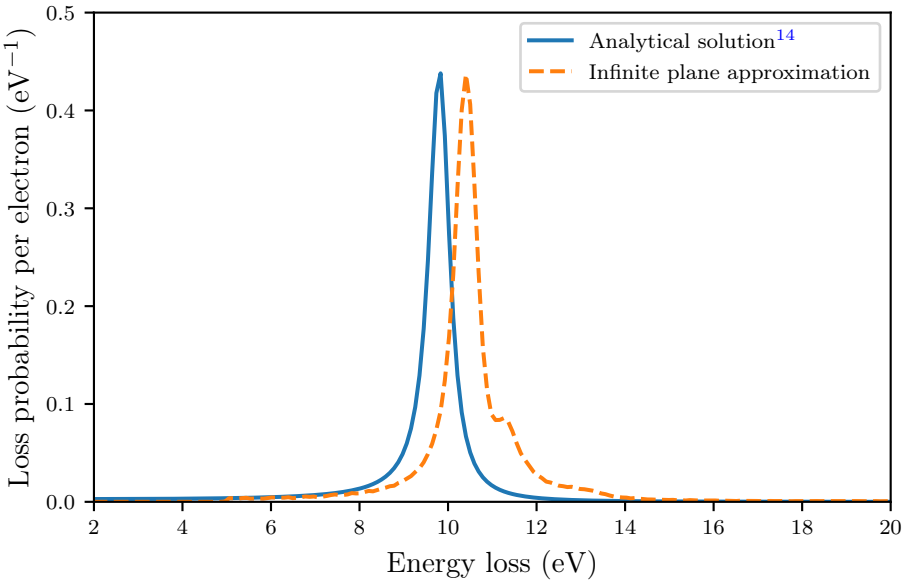

Figure 5. Loss probability distributions for a 500 eV electron passing at $b = 10.5$ nm from a $a = 10$ nm aluminium sphere. This figure compares the analytical solution (blue curve) to the result from the flat-plane approximation (orange). Note the good agreement in absolute value.

The situation is as follows. An electron starts infinitely far away from a sphere with radius a. It moves past the sphere, with closest radius of passing $b > a$, and goes on to infinity. García de Abajo[14] then gives an expression for the "loss probability", given per unit of transferred energy. Its integral is the total probability that the electron loses energy.

With the flat-plane approximation, we can replicate this situation in a Monte Carlo fashion. We start the electron sufficiently far away from the sphere, tracking its energy as it passes the sphere, recording its final energy when it has moved sufficiently far away. This gives a distribution that is directly comparable, both in the distribution of energy lost and in terms of absolute value, to the analytical result.

The analytical result predicts that the low-order plasmon modes dominate when the electron energy is large and the electron passes far away from the sphere. García de Abajo confirms this for the classic case of a 200 keV electron, and $(a, b) = (5, 6)$ nm or $(10, 12)$ nm. However, as mentioned, the much lower-energy electrons considered in this work barely interact with surface plasmons at such distances from the surface. They need to pass much closer to the surface. In the analytical result, the low-order modes are then suppressed, and higher-order modes become more important.

We show numerical results for the energy-loss distribution in figure 5. The situation is a 500 eV electron, passing a sphere with $a = 10$ nm at a distance $b = 10.5$ nm. The low-order modes in the analytical result are suppressed, and barely contribute to the peak in figure 5. Instead, the peak is caused by a combination of several higher-order modes. The amount of energy loss predicted by the analytical formula is slightly different from the flat-plane approximation. However, the agreement in absolute value is very good.

In conclusion, the amount of energy loss is slightly overestimated by the flat-plane approximation. However, the number of events is captured very well. The latter property is the most important for the purpose of SEM images.

3.3 Monte Carlo implementation

The Monte Carlo implementation is not as straightforward as it is for bulk inelastic scattering. For bulk inelastic scattering from equation (2), one needs to store two- and three-dimensional tables. The two-dimensional table contains a probability distribution of energy loss, for each electron energy of interest. The three-dimensional table contains, for each electron energy and energy lost, a probability distribution of the momentum loss.

Surface inelastic scattering also depends on the electron's distance and angle to the surface, adding two dimensions to the tables mentioned above. In addition, we now need to sample two degrees of freedom for the momentum transfer. The bottom line is a need for 4, 5 and 6-dimensional tables: too large to fit in our computer's memory.

Therefore, we make the simplification that an inelastic event only causes the electron to slow down. We then only need a 4-dimensional table to sample the energy loss given the original energy, distance and angle to the surface.

When an inelastic event takes place, a secondary electron is created moving in a uniformly-distributed random direction. Its energy is equal to the energy lost by the primary electron. If the primary electron is in vacuum, the SE is started on the mirrored side of the boundary, inside the material. We acknowledge that this model is very simplistic and that there is room for improvement.

What remains to be discussed is when an inelastic event takes place. Remember that the "mean free path" changes as a function of the electron's position. A random free path length sampled according to equation (1) is therefore only correct near the electron's starting position. This can be solved by introducing a "maximum step length" between successive scattering events. This maximum step length should be small enough, such that the mean free path barely changes over this distance. We have used 0.1 Å here, but a larger value is possible without significantly influencing the results.

If the free path sampled according to equation (1) is longer than this maximum, we travel precisely the maximum and sample a new free path length. This mechanism prevents steps between the "physical" elastic or inelastic events from getting too large, and guarantees that the inelastic mean free path is suitably updated along the electron trajectory. Salvat-Pujol *et al.*[15] do something similar, except their "null" event takes place stochastically with a mean free path $\lambda_{\min}$. This should lead to similar behaviour in the limit that $\lambda_{\min}$ is much smaller than the elastic or inelastic mean free paths[†].

4. RESULTS

4.1 Backscattered and secondary energy spectra

We present the simulated reflection energy loss spectrum (REELS) in figure 6. This was made for a 300 eV beam impinging perpendicularly on aluminium. Two simulations are shown: one with and one without surface effects enabled.

The energy spectrum without surface effects enabled is easily interpreted. The sharp peak at zero loss represents electrons reflected without losing energy. The strong peak at 15 eV represents electrons that have lost energy to a volume plasmon. Further peaks represent the excitation of multiple volume plasmons.

Enabling surface effects has a clear impact on the energy spectrum. The strong volume plasmon peak at 15 eV is reduced in absolute magnitude, and is joined by the surface plasmon at approximately 11 eV. Subsequent peaks are caused by the excitation of multiple surface and/or volume plasmons. Clearly, if the backscattered energy spectrum is of interest, it is important that surface plasmons are taken into account.

The corresponding energy spectrum for secondary electrons is presented in figure 7. The distinctive peaks in the energy loss spectrum of figure 6 are not visible. No additional "surface plasmon" peak is visible when surface effects are enabled in the simulation. This is because of our assumptions in the SE generation mechanism: SEs generated after surface plasmon decay are created inside the material and have to overcome the work function barrier to escape the material. The probabilistic transmission model mentioned in section 2 effectively smooths out any features in the SE energy spectrum as it exists inside the material.

4.2 Yields

When taking SEM images, one is not typically interested in the detailed energy spectrum. Instead, detected electrons are counted, with only a very crude energy filter to distinguish between "secondary" (< 50 eV) and

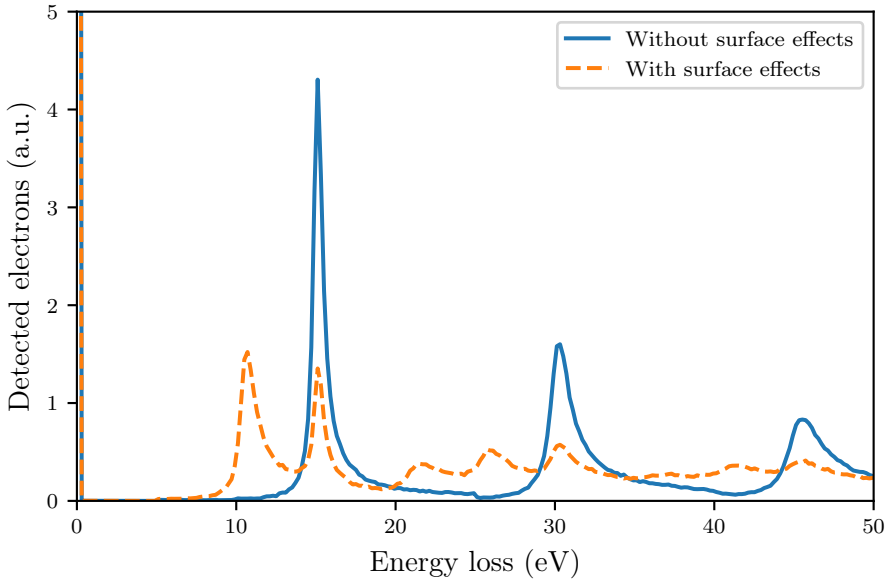

Figure 6. Energy loss spectrum, for a 300 eV beam on aluminium. Simulations with (orange curves) and without (blue) surface effects enabled are compared.

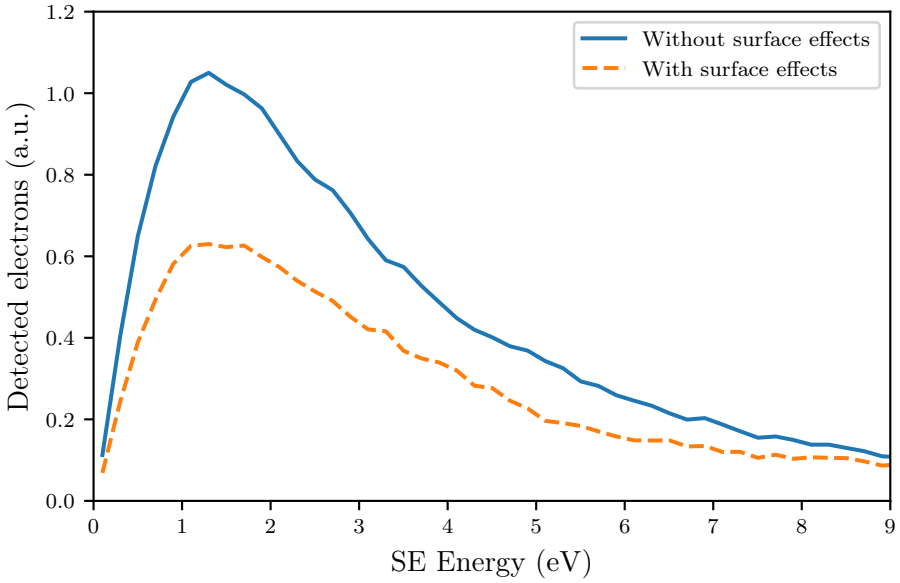

Figure 7. Secondary electron energy spectrum, for the same simulation as figure 6. Simulations with (orange curves) and without (blue) surface effects enabled are compared.

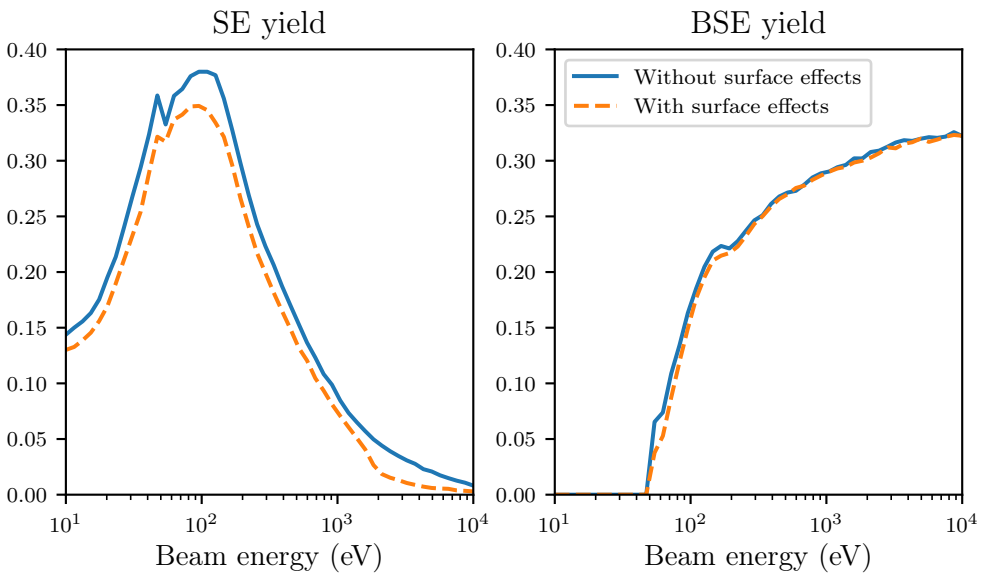

Figure 8. Simulated secondary (left) and backscattered (right) yields, for simulations with (orange curves) and without (blue) surface effects enabled. The material used is silicon. We emphasise that the yields shown here are very different than measured values.

"backscattered" ($> 50\,\text{eV}$) electrons. These yields—the average number of secondary or backscattered electrons per incident electron—are shown in figure 8 for a range of beam energies and silicon.

There is a large discrepancy between these simulated yields and typical measured data[16] (not shown). Measured SE yields for silicon tend to reach a maximum of around 1.2 at a beam energy of approximately 300 eV; BSE yields saturate at around 0.2. Typical Monte Carlo simulations,[3–6] while by no means perfect, tend to be more accurate, especially in the prediction of BSE yields. The fact that the present simulations do not predict accurate yields is not surprising, since we used a very crude single-oscillator model to represent the dielectric function, as well as some crude approximations regarding the generation of secondary electrons.

The fact that the yields are wrong in the absolute sense is not a cause for immediate concern. The goal of the present work is to study the influence of enabling surface effects. While the "silicon" in the present simulations does not represent real silicon very accurately, we do believe that qualitative changes to the SEM signal are captured correctly. In the following discussion, we will note any simulation results that we do not believe to be trustworthy.

We conclude that while the backscattered energy spectrum (figure 6) is significantly influenced by enabling surface effects, the BSE yield (figure 8) is not. In a way, the signal in figure 6 is redistributed to other losses, but the integral under the curve remains the same.

Note that figure 8 appears to indicate that the SE yield decreases slightly when surface effects are enabled. Due to the very crude assumptions made for the mechanism of SE generation, this result should not be trusted. It is possible that more accurate mechanisms for SE generation result in an increased yield when surface effects are enabled.

4.3 SEM image

We will now investigate the effect of introducing surface effects on a SEM image of a single silicon step (see figure 9). This step has circular rounded top and bottom corners to ensure smoothness. We vary the sidewall angle and electron beam energy. The electron beam is infinitely sharp, and we show only the SE signal.

[†]There appears to be a small error in Salvat-Pujol *et al.*, step 3a: $\lambda_{\text{min}}^{-1}$ should be replaced by $\lambda_{\text{min}}^{-1} + \lambda_{\text{e}}^{-1} + \lambda_{\text{i}}^{-1}$. This is likely to be a typo, since the reference they provide for the algorithm is correct.

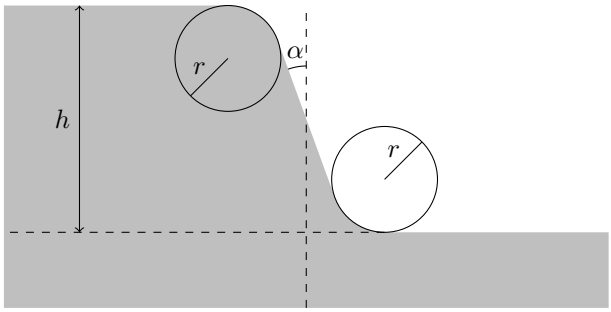

Figure 9. Step geometry. The shaded area represents the silicon. The top and bottom corners are circular, and the wall may be angled.

We want to compare simulations with surface effects enabled and with surface effects disabled. We apply a vertical offset and linear scaling to the absolute SE yield, such that the signals overlap away from the edge. This facilitates comparison of the signals near the edge.

We show the case of a vertical sidewall in figure 10. The step height is 20 nm and the corner radius is 5 nm, the beam energies are 300 eV and 500 eV. All SEM traces show the well-known enhancement of signal near the edge, which we will call the "edge blooming" effect in this work. When surface effects are enabled in the simulation, the SEM image taken at 300 eV shows a very sharp additional spike near the edge. This is a direct consequence of a somewhat pathological set of assumptions and parameters: the infinitely sharp electron beam travels at extremely close range ($x = 0.05$ nm) to the edge, and is oriented perfectly parallel to the edge. The electrons travel on the vacuum side and are able to efficiently excite surface plasmons, and secondary electrons, without being deflected.

No spike can be seen for 500 eV beam energy, though the SEM signal is slightly enhanced at $x = 0.05$ nm when surface plasmons are enabled. The fact that the spike is not present in the 500 eV linescan is due to the larger mean free path for these higher-energy electrons.

When the step height is increased to 40 nm (figure 11), a spike also appears in the 500 eV SEM signal. The spike for a 300 eV beam at a 40 nm step is even higher. The magnitude of this latter spike is unlikely to be physically accurate, because an incident electron can very efficiently create multiple SEs via surface coupling. Remember that a "surface event" does not deflect the primary electron in the present model. The slight deflection the primary electron suffers in reality would rapidly steer it out of the very narrow surface layer.

A 5° sidewall angle (figure 12) eliminates the observed spike. Instead, the SEM signal from the sidewall is somewhat enhanced when the electron beam is set to 300 eV. Surface effects make almost no difference under a 500 eV beam.

A feature with 1° sidewall angle (figure 13) holds few surprises given the other results. The signal from the sidewall-angle is enhanced, to a degree more extreme than seen in figure 12 but less than the spikes in figures 10 and 11. The simulation with surface effects enabled predicts that the signal at the sidewall exceeds the familiar "edge bloom" effect if the beam energy is low. As before, whether this is physically accurate is doubtful due to the contribution of multiple scattering events as well as the assumption that every surface plasmon decays to an electron.

The result in figure 13 is of interest to metrology. When surface effects are taken into account, the signal from the sidewall exceeds the "edge blooming" effect. This introduces a significant bias into the measured position of the edge.

There are multiple ways to measure the edge position in a SEM signal. A typical way is to take the position where the signal intensity is at 60 % between the minimum and maximum. If the edge position is measured in this way, figures 10, 11 and 12 correspond to a bias of 0.1 nm or less. In figure 13, however, the simulations with surface effects included position the edge 0.6 nm further to the right than the corresponding simulations without surface effects included.

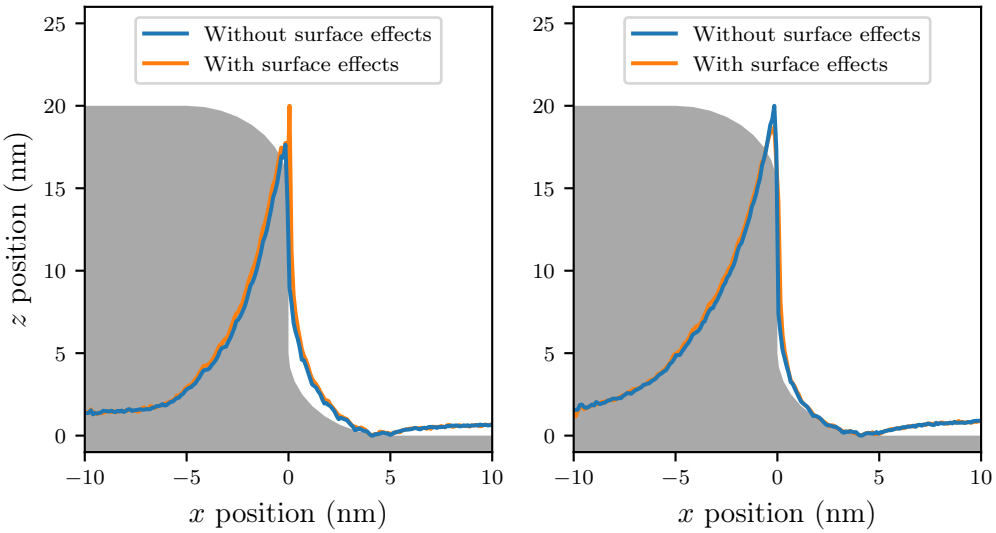

Figure 10. SEM signals for a geometry with $h = 20\,\text{nm}$, $r = 5\,\text{nm}$, $\alpha = 0°$. Simulations with (orange curves) and without (blue) surface effects enabled are compared. Left: beam energy 300 eV; right: beam energy 500 eV. The shaded area represents the silicon feature. Note that the feature appears skewed because the axes are not equally scaled.

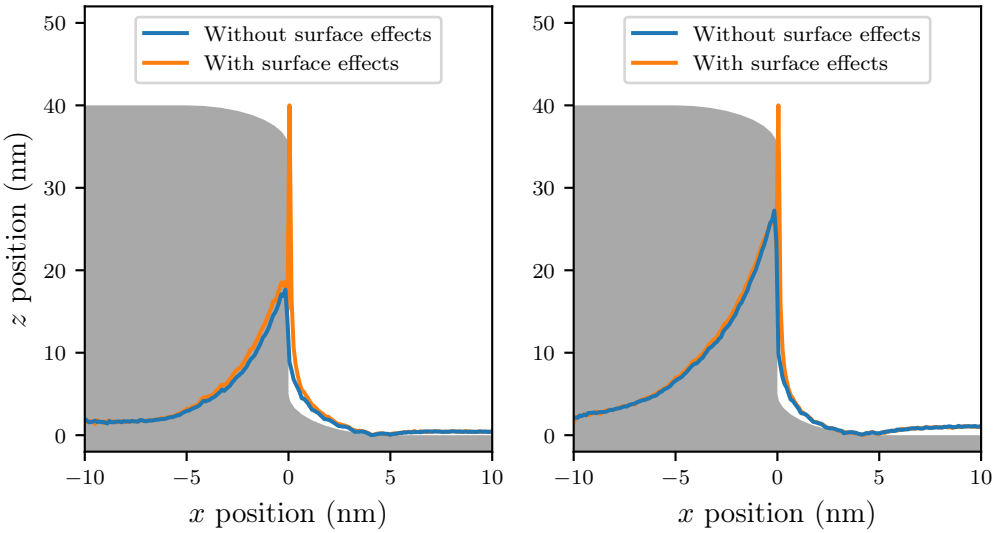

Figure 11. Same as figure 10, for $h = 40\,\text{nm}$.

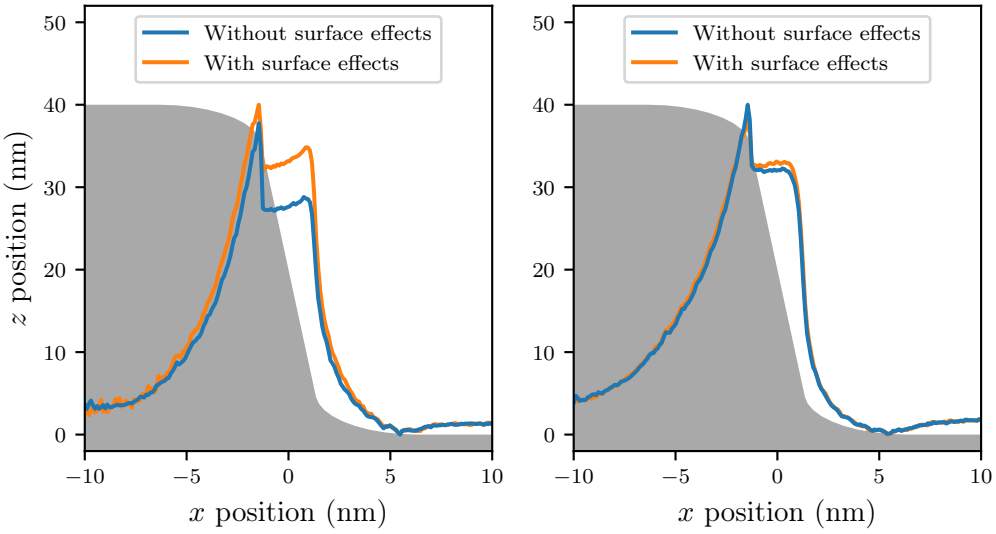

Figure 12. Same as figure 10, for $\alpha = 5°$, $h = 40\,\text{nm}$.

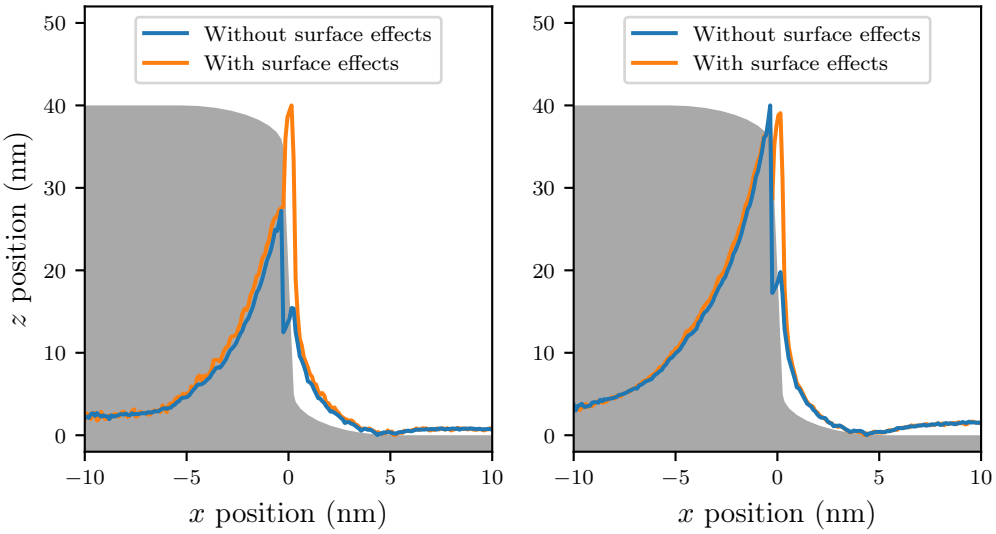

Figure 13. Same as figure 10, for $\alpha = 1°$, $h = 40\,\text{nm}$.

5. CONCLUSIONS

The results shown above can be summarised as follows. Inclusion of surface effects in a Monte Carlo simulation leads to

- virtually no change in BSE yield,
- a somewhat different SE yield (we do not trust the present results about the direction or magnitude),
- a changed BSE energy spectrum,
- a changed, but still mostly featureless, SE energy spectrum,
- a relative increase of the SE signal near a feature side-wall, which is largest for low landing energies.

Amongst others, we have assumed that incident electrons, upon coupling to a surface plasmon while in vacuum, do not change direction. We have also assumed that every surface plasmon decays to an electron-hole pair. These two assumptions lead to an overestimation of the amount by which the SE signal is increased near a side-wall. In some of the situations we showed, the SE signal from a wall exceeds the edge blooming effect that is typically observed near the top of a feature. Whether or not this happens in reality remains to be seen. It would be difficult to observe this effect directly: for example, taking into account the beam spot size and angle, as well as a sample's roughness, the "wall feature" in figure 13 will appear indistinguishable from the edge blooming effect.

If the enhancement of the signal from the sidewall angle is indeed as big as these simulations suggest, this can lead to a different assignment of the edge position when the SEM image is interpreted. Effectively, this position may shift from the "top" of the sidewall to the "bottom" side. One should be aware of this when comparing simulations to experiment.

Surface effects have a much less significant influence on the SEM signal near the rounded top and bottom corners of our feature. We acknowledge that our corner radius is much larger than what is typical. However, under the present physical assumptions, decreasing this radius does not lead to more interesting features in the SEM signal.

It is possible that more interesting features arise when the flat-plane assumption is lifted and Maxwell's equations are solved for the actual geometry of interest. However, given that our present model captures most of the interesting features, we do not expect the qualitative conclusions to change much. The only interesting feature we observe, for the purposes of CD-SEM metrology, is an enhancement in signal from the sidewall angle. A more thorough treatment may, therefore, not be worth the effort.

REFERENCES

[1] Frase, C. G., Buhr, E., and Dirscherl, K., "CD characterization of nanostructures in SEM metrology," *Measurement Science and Technology* **18**(2), 510–519 (2007).

[2] Mack, C. A. and Bunday, B. D., "Improvements to the analytical linescan model for SEM metrology," in [*Proceedings of SPIE*], Sanchez, M. I. and Ukraintsev, V. A., eds., **9778**, 97780A (2016).

[3] Villarrubia, J. S., Vladár, A. E., Ming, B., Kline, R. J., Sunday, D. F., Chawla, J. S., and List, S., "Scanning electron microscope measurement of width and shape of 10nm patterned lines using a JMONSEL-modeled library," *Ultramicroscopy* **154**, 15–28 (2015).

[4] Kieft, E. and Bosch, E., "Refinement of Monte Carlo simulations of electron–specimen interaction in low-voltage SEM," *Journal of Physics D: Applied Physics* **41**(21), 215310 (2008).

[5] Zou, Y. B., Khan, M. S., Li, H. M., Li, Y. G., Li, W., Gao, S. T., Liu, L. S., and Ding, Z. J., "Use of model-based library in critical dimension measurement by CD-SEM," *Measurement: Journal of the International Measurement Confederation* **123**(December 2017), 150–162 (2018).

[6] Verduin, T., Lokhorst, S. R., and Hagen, C. W., "GPU accelerated Monte-Carlo simulation of SEM images for metrology," in [*Proceedings of SPIE*], Sanchez, M. I. and Ukraintsev, V. A., eds., **9778**, 97780D (2016).

[7] Pijper, F. J. and Kruit, P., "Detection of energy-selected secondary electrons in coincidence with energy-loss events in thin carbon foils," *Physical Review B* **44**(17), 9192–9200 (1991).

[8] Mullejans, H., Bleloch, A. L., Howie, A., and Walsh, C. A., "Secondary-electron emission from magnesium oxide," *Philosophical Magazine Letters* **68**(3), 145–151 (1993).

[9] Scheinfein, M. R., Drucker, J., and Weiss, J. K., "Secondary-electron production pathways determined by coincidence electron spectroscopy," *Physical Review B* **47**(7), 4068–4071 (1993).

[10] Werner, W. S. M., Ruocco, A., Offi, F., Iacobucci, S., Smekal, W., Winter, H., and Stefani, G., "Role of surface and bulk plasmon decay in secondary electron emission," *Physical Review B - Condensed Matter and Materials Physics* **78**(23), 1–4 (2008).

[11] Mott, N. F., "The Scattering of Fast Electrons by Atomic Nuclei," *Proceedings of the Royal Society A: Mathematical, Physical and Engineering Sciences* **124**(794), 425–442 (1929).

[12] Salvat, F., Jablonski, A., and Powell, C. J., "Elsepa - Dirac partial-wave calculation of elastic scattering of electrons and positrons by atoms, positive ions and molecules," *Computer Physics Communications* **165**(2), 157–190 (2005).

[13] Schreiber, E. and Fitting, H.-J., "Monte Carlo simulation of secondary electron emission from the insulator SiO2," *Journal of Electron Spectroscopy and Related Phenomena* **124**(1), 25–37 (2002).

[14] García de Abajo, F. J., "Optical excitations in electron microscopy," *Reviews of Modern Physics* **82**(1), 209–275 (2010).

[15] Salvat-Pujol, F. and Werner, W. S., "Surface excitations in electron spectroscopy. Part I: Dielectric formalism and Monte Carlo algorithm," *Surface and Interface Analysis* **45**(5), 873–894 (2013).

[16] Joy, D. C., "A database on electron-solid interactions," *Scanning* **17**(5), 270–275 (1995).